

Article

Evolution and Evaluation of Aesthetic Properties in Weathering Steel Accelerated Patinas: The Role of Lepidocrocite

Ana Crespo ^{1,4,*} , Gloria Pérez ⁵ , José A. Jiménez ², Irene Llorente ³, Sagrario Martínez-Ramírez ¹ , Emilio Cano ⁴  and Iván Díaz ⁴

¹ Departamento de Espectroscopía Nuclear, Vibracional y de Medios Desordenados, Instituto de Estructura de la Materia, Consejo Superior de Investigaciones Científicas (IEM, CSIC), 28006 Madrid, Spain; sagrario.martinez@csic.es

² Departamento de Metalurgia Física, Centro Nacional de Investigaciones Metalúrgicas, Consejo Superior de Investigaciones Científicas (CENIM, CSIC), 28040 Madrid, Spain; jimenez@cenim.csic.es

³ Laboratorio de Difracción de Rayos X, Centro Nacional de Investigaciones Metalúrgicas, Consejo Superior de Investigaciones Científicas (CENIM, CSIC), 28040 Madrid, Spain; irene@cenim.csic.es

⁴ Departamento de Ingeniería de Superficie, Corrosión y Durabilidad, Centro Nacional de Investigaciones Metalúrgicas, Consejo Superior de Investigaciones Científicas (CENIM, CSIC), 28040 Madrid, Spain; ecano@cenim.csic.es (E.C.); ivan.diaz@csic.es (I.D.)

⁵ Departamento de Materiales, Instituto de Ciencias de la Construcción Eduardo Torroja, Consejo Superior de Investigaciones Científicas (IETcc, CSIC), 28033 Madrid, Spain; gperezaq@ietcc.csic.es

* Correspondence: a.crespo.i@csic.es

Abstract: Weathering steels are widely used in civil engineering, architecture and contemporary art due to their mechanical properties, their enhanced resistance to atmospheric corrosion as well as their aesthetic properties. Artists and blacksmiths often apply chemical treatments to obtain the appealing colors of a patina in a shorter period of time. However, the development of an accelerated patina may have an effect on the final appearance and color of the surface. With the aim of evaluating differences in color and studying the evolution of the surface, eight accelerated patinas were made and exposed to the atmosphere for periods of time of up to 24 months and were compared to a natural patina. The characterization studies showed the presence of lepidocrocite on the surface. A close inspection of the X-ray diffraction patterns showed the displacement of the (020) lepidocrocite reflection and asymmetric broadening of selective lines of this phase that were associated to stacking and twins faults, respectively. These faults decrease with the exposure time and are related to a maximum at 630 nm in the reflectance spectrum and the stabilization of the b* coordinate (yellow color). The colors of the accelerated patinas differ from the natural patina at short exposure times. However, they tend to converge at longer exposure times.

Keywords: weathering steel; sculpture; corrosion; color; contemporary art; conservation-restoration; cultural heritage; Raman spectroscopy; X-ray Diffraction; lepidocrocite



Citation: Crespo, A.; Pérez, G.; Jiménez, J.A.; Llorente, I.; Martínez-Ramírez, S.; Cano, E.; Díaz, I. Evolution and Evaluation of Aesthetic Properties in Weathering Steel Accelerated Patinas: The Role of Lepidocrocite. *Metals* **2022**, *12*, 977. <https://doi.org/10.3390/met12060977>

Academic Editor: Hannu Hänninen

Received: 10 May 2022

Accepted: 4 June 2022

Published: 7 June 2022

Publisher's Note: MDPI stays neutral with regard to jurisdictional claims in published maps and institutional affiliations.



Copyright: © 2022 by the authors. Licensee MDPI, Basel, Switzerland. This article is an open access article distributed under the terms and conditions of the Creative Commons Attribution (CC BY) license (<https://creativecommons.org/licenses/by/4.0/>).

1. Introduction

Weathering steels (WS) are classified as high strength low alloy steels (HSLA) with a quantity of carbon less than 0.2% and with a total amount of alloy elements, such as Cu, Cr, Ni and Mn lower than 3–5% in weight [1]. Their commercial name Cor-Ten © refers to the atmospheric corrosion resistance and tensile strength of WS. Their corrosion resistance arises from the development of a protective corrosion layer that is adherent, compact and dense [2,3] with self-healing properties [4], which allows for the use of WS outdoors without the necessity of being painted [5].

For its formation, the protective corrosion layer needs long exposure times [6] to wetting and drying cycles [7] and also specific atmospheric conditions, such as, the practical absence of chloride ions [8]. The development of the protective corrosion layer and the appealing colors of the rust, together with the high performance of WS are the reasons why

WS were widely used in civil engineering, architecture and contemporary art [9]. The use of WS in sculpture started in the 1960s [10], when artists, concerned about the conservation of their artwork, started to look for new materials for outdoor exposure with the aim of lasting longer. The manufacture of artworks in WS is usually performed by sheets or plates bent and welded [11].

These installations usually take the form of large-scale pieces of art installations, which involves high weight as well and are placed outdoor in different environments, such as parks, gardens, streets or even in the desert [12]. It is also very common that sculptors and blacksmiths apply chemical treatments in order to develop an accelerated patina on metal surfaces, which are later exposed to the environment. The reason for the use of accelerated patinas is not only to obtain the bright colors of the patina in a short period of time; however, it constitutes an essential part of the creative investigation process of the artists in order to develop a patina according to their aesthetic and artistic creation [13].

For outdoor sculpture, the inevitable effects of environment complicate conservation tasks, being maintenance the most suitable strategy [14]. As WS is a material with enhanced resistance to atmospheric corrosion, little attention has been paid to the conservation of this material, even though some artworks have suffered alarming damage over the last forty years [14]. Interventions in WS are usually performed only when corrosion damage is catastrophic and removal or replacement is needed.

The replacement of some of the parts of the sculpture and the elimination of graffiti with abrasive methods usually involves the application of chemical treatments to develop accelerated patinas as described by Chemello et al. in [15]. As for works of art, the development of accelerated patinas on the metal surface exerts influence over the aesthetic properties of the artwork, since each chemical treatment develops different compounds and textures to the patinas.

Over the last few years, different works have been published focusing on the conservation of WS sculpture. Some authors characterize the corrosion products composition [16–18] and others evaluate the electrochemical properties of the patina [19–21]. As for the aesthetic properties, Dauksys et al. [22] evaluated the effect of NaCl and Na₂SO₄ solutions in the color and texture of WS surfaces under cyclic temperature changes. In addition, Travassos et al. [23] described the effect of different exposure season on the appearance of WS. However, color measurements are rarely performed, even though they could show signs of the deterioration of artworks [21].

As was mentioned above, accelerated patination treatments is another factor that has influence on the final color and appearance of a patina. Although the application of chemical compounds to the surface of WS to obtain accelerated patinas is common practice, there are no studies dealing with the effect that these treatments may have on the aesthetic properties of the patinas.

In this work, we present a compilation of information on widely used accelerated patination treatments for WS. The evolution of the aesthetic properties of these patinas, as well as the characterization of the corrosion products, were monitored up to 24 months of exposure to the atmosphere of Madrid (Spain). A classification of the accelerated patinas was conducted regarding their color coordinates L*, a* and b*. A new methodology for color analysis based on fitting is proposed.

2. Materials and Methods

2.1. Sample Preparation

Commercial WS sheets were cut into coupons of 11 × 6 cm² area whose composition was determined by atomic emission spectroscopy with SPECTROMAXx equipment (SPECTRO Analytical Instruments GmbH, Kleve, Germany). The sulfur and carbon content was analyzed by infrared absorption with Leco model CS230 (Leco Corporation, St. Joseph, MI, USA). The chemical composition of the WS is shown in Table 1.

Table 1. Chemical composition in % of weathering steel used for experimental samples.

Element	Fe	C	Si	Mn	P	S	Cu	Cr	Ni	Al
%	97.453	0.091	0.60	0.42	0.109	0.0123	0.302	0.807	0.181	0.025

The coupons were previously sandblasted using Al₂O₃ (size 297–420 μm) under 0.5 MPa to completely remove the oxide layer formed during hot rolling and obtain a surface state ASa3 (white metal with no pollutants), in accordance with the Swedish standard SIS 05 5900. Then, they were cleaned with distilled water, ethanol and acetone in consecutive ultrasound baths during one minute each to remove pollutants.

In order to prepare the WS coupons as closely as possible to real WS artwork, it was essential to reproduce the working methods that artists and blacksmiths apply in their studios. Therefore, the selection of chemical treatments applied to obtain the accelerated patinas (see Table 2) was chosen according to previous interviews with sculptors and blacksmiths. The aim of the interviews was to compile information about their work techniques with WS and to unify the information for a reproducible methodology.

Table 2. Chemical treatments selected from interviews to obtain accelerated patinas on WS.

Treatment	Molarity (mol/L)
FeCl ₃	1.47
Fe(NO ₃) ₃	0.99
H ₂ SO ₄	1.87
HCl	1.01
HNO ₃	1.09
H ₂ O ₂	9.70
CH ₃ COOH	1.74
NaHSO ₃	1.42

In total, 27 professionals in the field of WS contemporary art were consulted. The solutions of the different chemical treatments were applied to the surface of the WS coupons following the indications of the sculptors and blacksmiths. The application was performed with a brush covering the entire surface. After drying for 24 h, all the samples were cleaned under wet and dry cycles with abundant distilled water for five days (approximately 50 mL/cm² each 24 h).

After the formation of the accelerated patinas, the WS coupons were exposed to the atmosphere of Madrid (Spain) the 21 of March 2017. The climate of Madrid has a dry and mild weather according to data provided by the State Meteorological Agency, with average temperature variations from 5 °C in the winter and 28 °C during summer (Figure 1). The atmosphere was classified as C2 according to the ISO 9223. Coupons were displayed on a stretcher frame following the specifications of ASTM G50 and recommendations in [24,25].

In addition to the accelerated patinas, coupons without chemical treatments, i.e., bare WS, were also exposed. They were included in the study with the aim of having a patina exclusively developed by atmospheric corrosion, called a natural patina. This natural patina will be used as a reference to measure the changes of the accelerated patinas. The present study compiles results up to 24 months of atmospheric exposure. Monitoring was done at zero time, i.e., prior to atmospheric exposure, and at 3, 6, 12 and 24 months of exposure time.

2.2. Color Measurements

Color analysis was performed with Konica Minolta CM 700D spectrophotometer (Konica Minolta Sensing Europe B.V., Nieuwegein, The Netherlands) with D65 as standard illuminant and d:8° geometry conditions. Analysis was done over the entire surface of the coupons in a uniform distribution with a template. In total, 23 points were measured by triplicate, and mean values were calculated. Reflectance spectra of the patinas were

measured in the wavelength range from 400 to 700 nm, and the color coordinates were calculated in the CIE L*a*b* color space. This color space model represents a sphere where L*, a* and b* are the z, x and y coordinates, respectively.

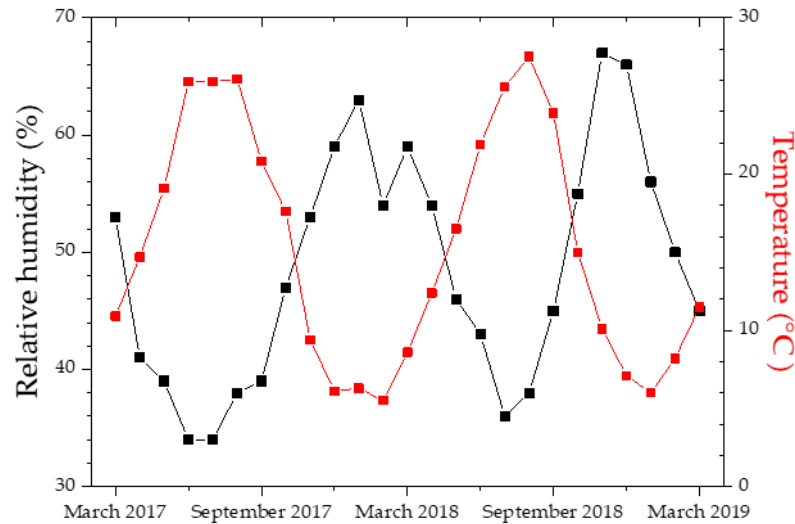


Figure 1. Average relative humidity and temperature of the atmosphere of Madrid during the exposure time. Data provided by the State Meteorological Agency.

The a* coordinate varies between −60 and +60, with negative values for green and positive values for red. The b* coordinate also varies between −60 and +60, where negative is for blue and positive is for yellow. Finally, the L* coordinate indicates lightness, being 0 for black and 100 for white. A more descriptive model than L*a*b* is L*C*h* [26], where L* corresponds to luminosity (the same as in L*a*b*), C is the chroma, and h refers to the hue. CIE L*a*b* and CIE L*C*h* can be easily converted from one to another with the formulas (Equation (1)) and (Equation (2)) (see Figure 2).

$$C = \sqrt{a^{*2} + b^{*2}} \tag{1}$$

$$h = \tan^{-1}(b^*/a^*) \tag{2}$$

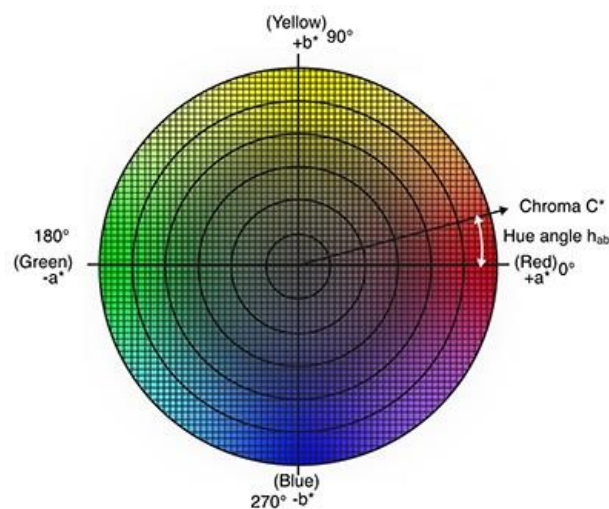


Figure 2. Graphical interpretation of chroma and hue in the color sphere for a* and b* coordinates section. Image from <https://sensing.konicaminolta.us/us/blog/understanding-the-cie-lch-color-space/> (accessed on 4 April 2022).

As color perception is a subjective matter, color adjectives can be confusing. With the purpose of unifying concepts, an image adapted from the Konica Minolta manual is shown (Figure 3), where adjectives of color depending on the L^* , a^* and b^* values are described.

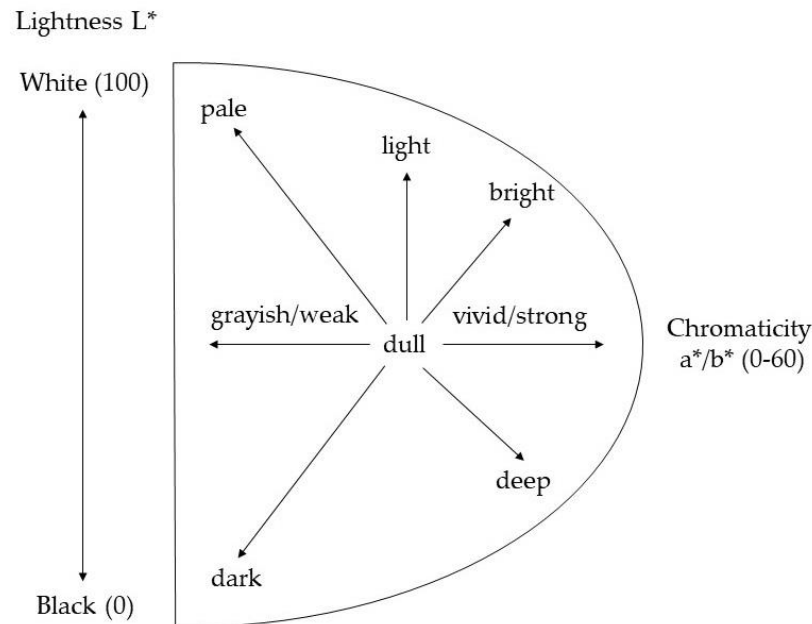


Figure 3. Adjectives of color according to L^* , a^* and b^* values. Adapted from the Konica Minolta CM700D manual <https://www.konicaminolta.com/instruments/knowledge/color/part1/07.html> (accessed on 4 April 2022).

2.3. Evaluation of Color Differences and Similarities: ΔE and Hue

Color perception involves complex processes in the observer as the result of contrast and memory effect. Therefore, objective color measurements are of a great help to obtain quantitative results [26]. There are several formulas to calculate color differences but the most widely used is ΔE (Equation (3)), which was proposed by CIE committee in 1976.

$$\Delta E = \sqrt{\Delta L^{*2} + \Delta a^{*2} + \Delta b^{*2}} \quad (3)$$

where $\Delta L^* = L^*_1 - L^*_2$, $\Delta a^* = a^*_1 - a^*_2$ and $\Delta b^* = b^*_1 - b^*_2$.

ΔE (Equation (3)) compares only two $L^*a^*b^*$ coordinates at the same time ($L^*_1a^*_1b^*_1$ and $L^*_2a^*_2b^*_2$). With this formula, it is difficult to make a comparison between a higher number of coordinates simultaneously.

To solve this limitation, a simpler method of data analysis is proposed to evaluate differences in chroma or hue for a higher number of collected data. If looking carefully, C formula (Equation (1)) represents the modulo of a straight line from the center of the sphere to the points defined by the a^* and b^* coordinates, while hue (Equation (2)) represents its angle (Figure 2). In this way, when the a^* and b^* coordinates fit to a semicircle, collected data will have similar chroma but different hues. On the contrary, when they fit to a straight line, collected data will have similar hue but different chroma.

In this work, mean values of a^* and b^* coordinates were fitted to a straight line with the formula (Equation (4)), where h is the hue. The value h describes yellowish colors when higher than 1 and reddish colors when lower than 1. This formula has zero intercept to force the straight line to start at the center of the sphere. Standard error and Pearson's coefficient was calculated to study the evolution of color differences with the passage of time.

$$a^* = h \cdot b^* \quad (4)$$

2.4. Micro-Raman Analysis

Surface analysis spectra were performed with a RM 2000 Renishaw Raman microscopy (Renishaw plc, Old Town, Wotton-under-Edge, Gloucestershire, UK) equipped with a laser at 633 nm with a spot diameter of 1 μm , a Leica microscope coupled and a CCD camera electrically refrigerated. Additionally, to compare surface images with Raman spectrum, confocal Raman microscope Renishaw Invia (Renishaw plc, Old Town, Wotton-under-Edge, Gloucestershire, UK) equipped with a Leica microscope and an electrically refrigerated CCD camera was used.

Laser excitation lines were provided by a diode laser (785 nm) and frequencies were calibrated with silicon. The laser power was controlled at 2.5 mW for a 633 nm laser and 0.2 mW for a 785 nm laser in order to avoid thermal transformation [27,28]. Spectra were collected with 10 s of integration time and one to five accumulations to improve the signal-noise ratio. In order to unify the information across the surface of the patina, the same template for color analysis was used in the Raman spectroscopy focused on three different areas. However, both techniques analyzed a different area size.

2.5. Optical Microscope

Images of the surface were taken with a Stereo microscope Nikon SMZ800N (Nikon Instruments Europe B.V., Amsterdam, The Netherlands) equipped with a digital camera with Sony IMX 236 sensor (Nikon Instruments Europe B.V., Amsterdam, The Netherlands). With the aim of unifying information, the same template as in color and Raman spectroscopy was used. The images shown in this work belong to the central zone of the sample and $3.85\times$ magnification.

2.6. X-ray Diffraction

XRD measurements were performed with Co radiation ($\lambda = 1.78897 \text{ \AA}$) using a Bruker AXS D8 advance diffractometer (Bruker AXS GmbH, Karlsruhe, Germany) equipped with a Goebel mirror and a LynxEye linear detector. XRD data were collected using a conventional $\theta/2\theta$ mode over a 2θ range from 10 to 80° with a step width of 0.02° and a counting time of 1 s per step. Diffraction patterns were refined by the Rietveld method using the space group and crystallographic information for lepidocrocite, and goethite obtained from Pearson's Crystal Structure database [29]. A corundum reference sample was measured under the same experimental conditions to eliminate the instrumental contribution to peak broadening.

XRD data refinement was performed with the version 4.2 of the Rietveld analysis program TOPAS (Bruker AXS GmbH, Karlsruhe, Germany). The refinement protocol used has included the major parameters, such as the background, zero displacement, the scale factors, the peak breadth and the unit cell parameter parameters. Microstructural parameters, such as the crystallite size and microstrain, were simultaneously determined from line broadening of the diffraction patterns by the double Voigt approach [30], and the shifting of reflections was evaluated from the deviation of the diffraction angle from the theoretical Bragg position.

3. Results

3.1. Color Analysis

3.1.1. Color Evolution of the Natural Patina

After 3 months of atmospheric exposure a thin rust patina is formed with yellowish tone (Figure 4a). The surface turned to an apparently darker patina at 6 months of exposure time (Figure 4b). After 12 months of atmospheric exposure, a thick rust patina developed that was very similar in its aspect to the 24 month patina (Figure 4c,d), which was heterogeneous under the microscope with yellow and brown tones.

Table 3 shows the chromaticity (a^* and b^*) and lightness (L^*) mean values obtained in the CIE $L^*a^*b^*$ color space for the natural patina (without chemical treatment of patination) after 3, 6, 12 and 24 months of exposure to the Madrid atmosphere.

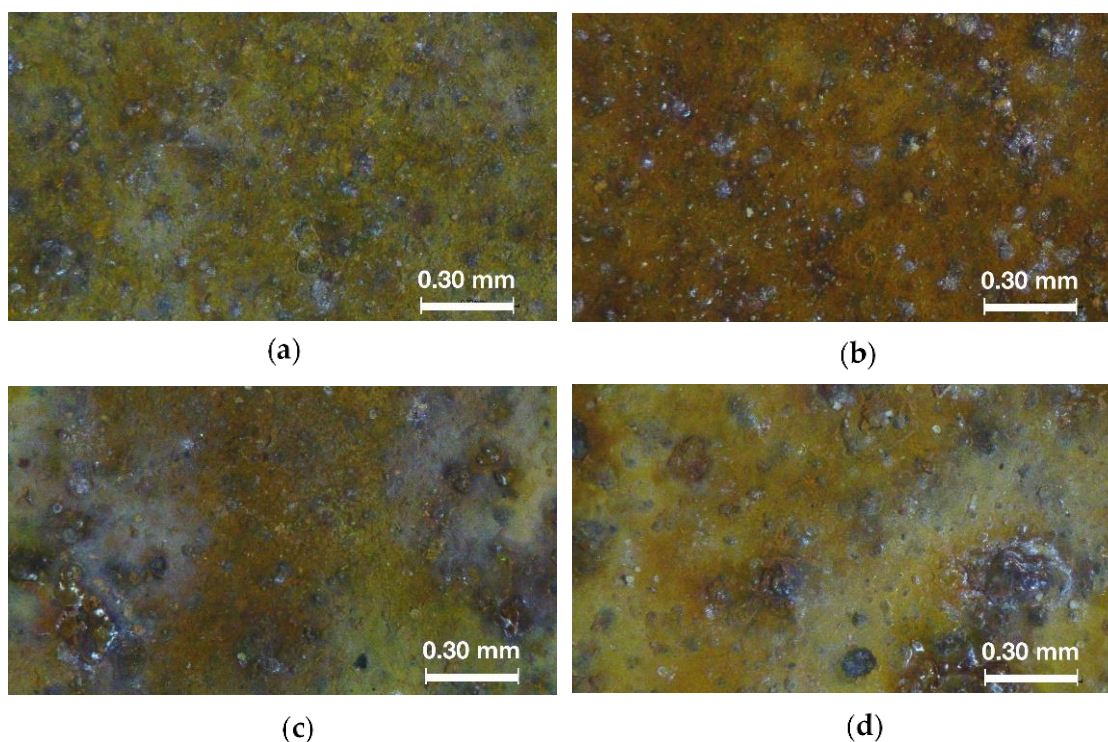


Figure 4. Optical microscope images of the natural patina developed after different exposure time to the Madrid atmosphere: (a) 3 months; (b) 6 months; (c) 12 months; and (d) 24 months.

Table 3. Evolution of the L^* , a^* and b^* coordinates of the natural patina with time at 95% confidence intervals.

Time	L^*	L^* Error	a^*	a^* Error	b^*	b^* Error
3 months	33.4	0.3	15.4	0.2	23.7	0.4
6 months	28.7	0.5	17.1	0.3	23.3	0.6
12 months	33.1	0.4	14.8	0.2	19.6	0.5
24 months	33.2	0.6	15.7	0.3	19.7	0.7

L^* = lightness; a^* = green ($-a^*$) and red ($+a^*$) component; b^* = blue ($-b^*$) and yellow ($+b^*$) component.

The L^* coordinate remains constant throughout the exposure time with the exception at 6 months, where it has a drop that recovers after 12 months. This effect is also appreciated in the optical microscope images in Figure 4, where a darkening of the natural patina is observed.

The a^* coordinate (red component) has an increase after 6 months of exposure time and recovers its initial value after 12 months. Regarding the b^* coordinate (yellow component), it remains constant during the first 6 months of atmospheric exposure. Then, it decreases sharply after 12 months and remains constant up to 24 months. The b^* values are higher than the a^* values at all exposure times, indicating yellow hue of the patina.

The decrease in the luminosity L^* at 6 months of atmospheric exposure is related to a drop in reflectance over the entire wavelength range from 400 to 700 nm (Figure 5). After 12 months of exposure, the reflectance spectrum shows a maximum at 630 nm (orange color), which remains after 24 months. The position of the maximum was determined by calculating the first derivative of the spectrum.

3.1.2. Color Evolution of Accelerated Patinas

The artificial patinas developed by accelerated chemical treatments at zero time, i.e., prior to their exposure to the Madrid atmosphere, have different aesthetic properties as can be seen in Figure 6 and the Supplementary Material.

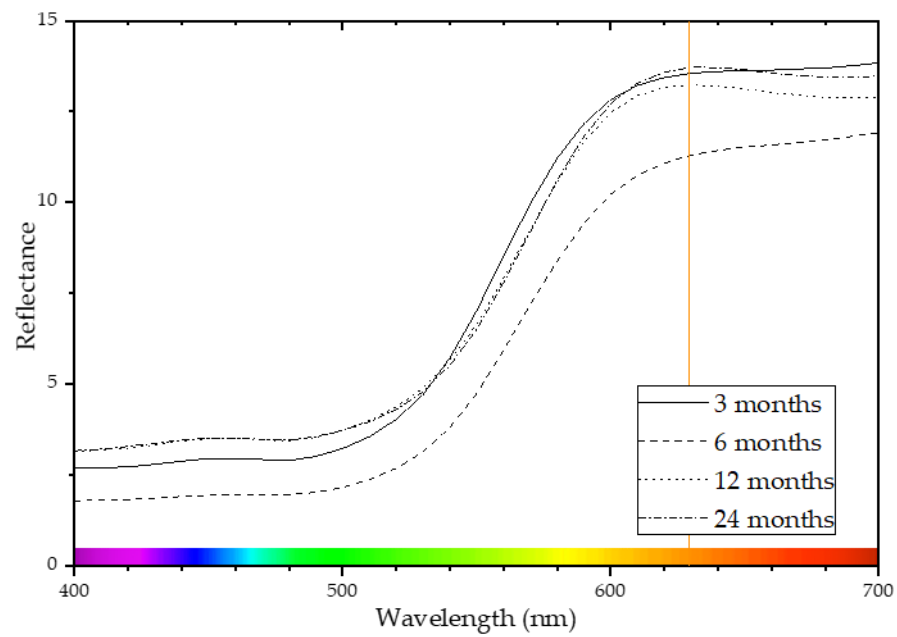


Figure 5. The reflectance spectra of the natural patina developed after different times of exposure to the Madrid atmosphere.

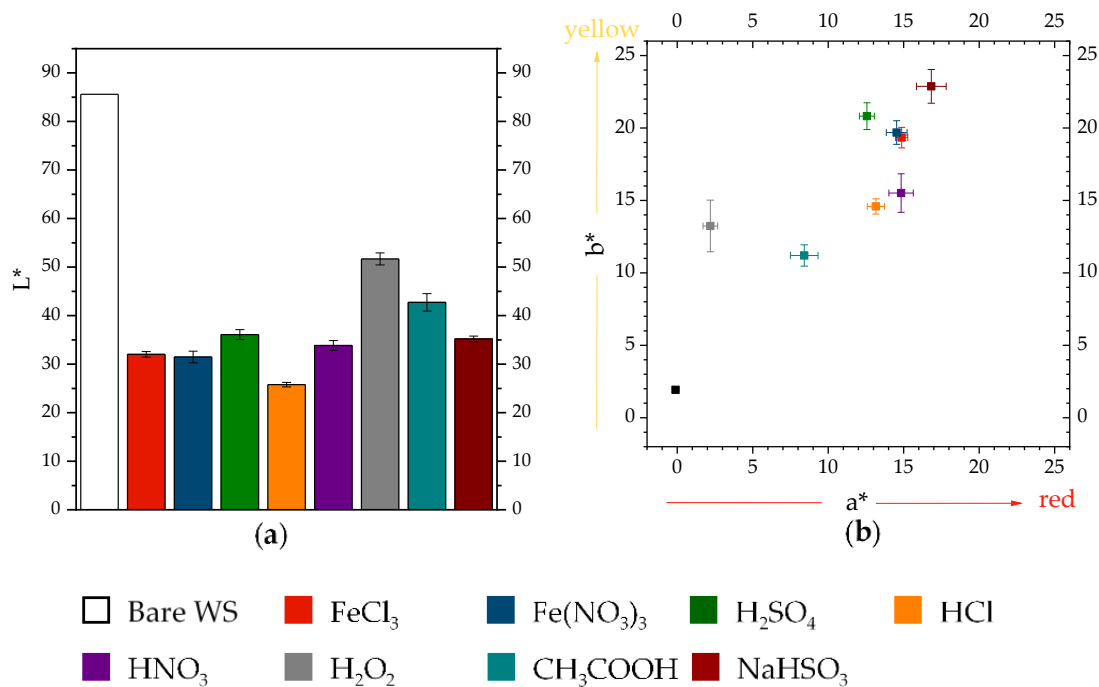


Figure 6. Lab values of the bare metal and the accelerated patinas at zero time: (a) L* value and (b) a* versus b* values.

The chemical treatments of FeCl₃ and Fe(NO₃)₃ develop similar patinas regarding their L* (lightness), a* (red) and b* (yellow) values. The patinas obtained after the application of H₂SO₄ and NaHSO₃ are lighter and brighter according to the definitions introduced in Figure 3, while the chemical treatments of HCl and HNO₃ make the patinas darker and deeper. Finally, the chemical treatments of H₂O₂ and CH₃COOH have a lower effect on the WS surface as they are not very corrosive treatments. They barely generate a corrosion layer, and thus the color properties are greatly affected by bare metal. However, the hue (Equation (2)) of each patina is different since it depends on the relative values of a* (red) and b* (yellow).

After 24 months of atmospheric exposure, the aesthetic properties of artificial patinas tend to converge (see Figure 7). L^* coordinate shows similar values for all the accelerated patinas, which are, in turn, very similar to the natural patina.

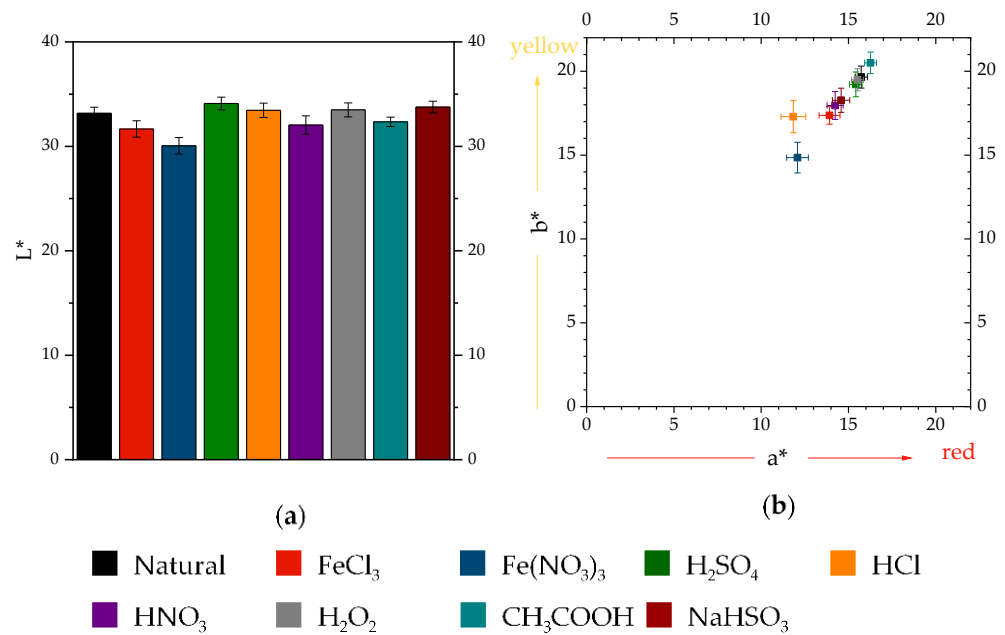


Figure 7. Lab values of the accelerated patinas after 24 months of exposure to the Madrid atmosphere: (a) L^* value and (b) a^* versus b^* values.

Similarly, the a^* and b^* values for each artificial patina are similar to each other as well as to those of the natural patina. The exception is the patina formed with $Fe(NO_3)_3$, which has notably lower a^* and b^* values—that is, weaker colors. The patina created with HCl treatment has similar values of L^* (lightness) and b^* (yellow) coordinates; however, the value of a^* (red) is lower, meaning that the hue of the patina is different.

3.1.3. Color Differences and Similarities

To compare $L^*a^*b^*$ values between natural and accelerated patinas and to study the evolution of differences over time, ΔE formula (Equation (3)) was used (Figure 8).

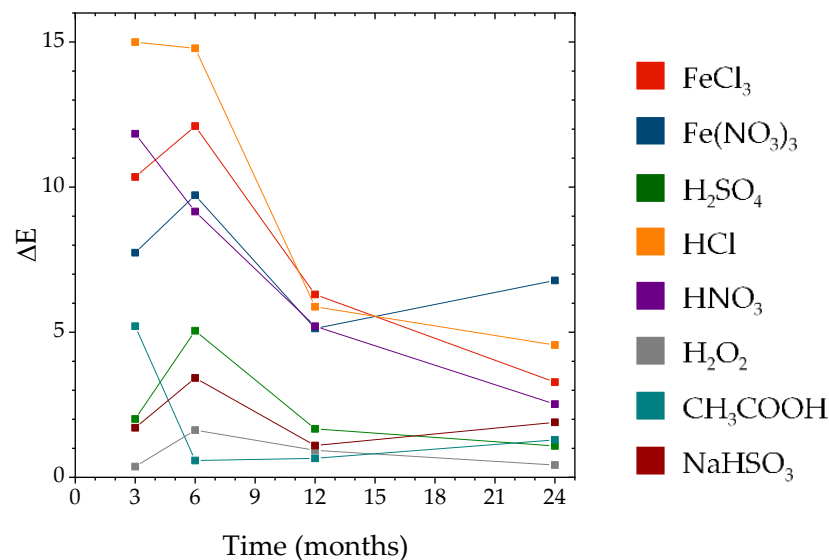


Figure 8. ΔE values comparing natural patina with accelerated patinas over time for 24 months period of atmospheric exposure.

Regarding the evolution of the ΔE values, after 3 and 6 months of atmospheric exposure the patination treatments have a great influence on the color properties of the patina. After 12 months of exposure time there are two defined groups: the comparable with the natural patina and the non-comparable; however, differences in color weaken with the passage of time. After 24 months, color differences tend to reduce. Higher differences are found for the patina developed with $\text{Fe}(\text{NO}_3)_3$, where the lower values a^* and b^* (Figure 7b) give rise to a grayish orange patina.

In the WS patinas studied, the graphical distribution of the data reveals similar hues as can be seen in Figure 9. In order to evaluate differences in hue over time, a lineal regression of the a^* and b^* coordinates was performed at different exposure times (Table 4). Pearson's coefficient and standard error were calculated to measure the lineal correlation between the data.

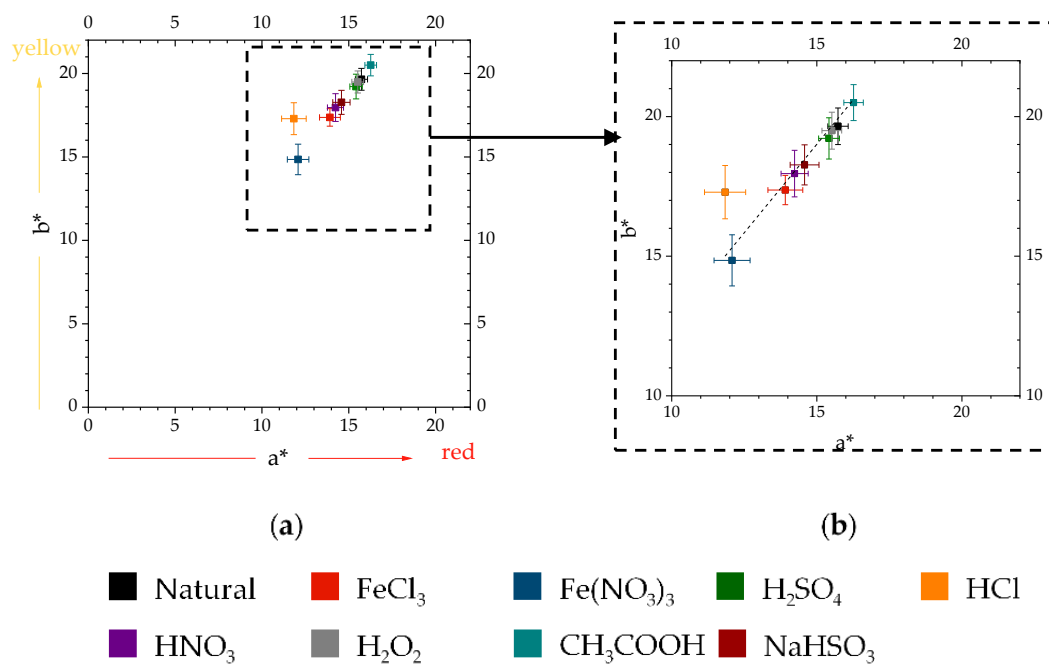


Figure 9. (a) The a^* and b^* values of the natural patina and the accelerated patinas after 24 months of atmospheric exposure and (b) amplification of the data, including a lineal regression with a zero intercept.

Table 4. Lineal regression fitting forcing to a zero intercept for accelerated patinas at zero time (prior to atmospheric exposure) and for a natural patina as well as accelerated patinas after different exposure times.

Months	Slope	Standard Error	Pearson's r
Zero time	1.32	0.13	0.9692
3	1.32	0.08	0.9859
6	1.28	0.06	0.9922
12	1.26	0.03	0.9981
24	1.27	0.02	0.9990

3.2. Raman Spectroscopy

The most common iron compounds identified in the literature in WS rust due to atmospheric corrosion are lepidocrocite, goethite, akaganeite, ferrihydrite (oxi-hydroxides), magnetite, maghemite and hematite [24,25,31–33]. In WS samples exposed to the Madrid atmosphere, lepidocrocite was identified in all patinas, natural and accelerated, and at all exposure times. Additionally, goethite and akaganeite were characterized for some of the accelerated patinas (Table 5).

Table 5. Oxi-hydroxides identified by Raman spectroscopy in the surface of WS patinas (natural and accelerated patinas) at zero time and after 3, 6, 12 and 24 months of exposure in the urban atmosphere of Madrid.

Treatment	Zero Time	3 Months	6 Months	12 Months	24 Months
Natural	-	L	L	L	L
FeCl ₃	L, A	L, A	L, A	L, A	L, A
Fe(NO ₃) ₃	L, G	L, G	L, G	L, G	L, G
H ₂ SO ₄	L	L	L	L	L
HCl	L, A	L, A	L, A	L, A	L
HNO ₃	L, G	L, G	L, G	L	L
H ₂ O ₂	L	L	L	L	L
CH ₃ COOH	L	L	L	L	L
NaHSO ₃	L	L	L	L	L

L = lepidocrocite; G = goethite; and A = akaganeite.

Akaganeite is an oxi-hydroxide commonly found in marine atmospheres. Therefore, since Madrid is far from the coast, its presence is due to the high concentration of chloride ions from the chemical treatments of FeCl₃ and HCl. Goethite is easily identified in accelerated patinas developed with nitrite ions (Fe(NO₃)₃ and HNO₃); however, as with akaganeite, the identification of this compound becomes more difficult over time.

3.3. X-ray Diffraction

The phase present in the XRD patterns were identified using the JCPDS data base. As expected, the XRD patterns of the natural patinas exposed to the atmosphere for periods of time of up to 24 months show the presence of lepidocrocite (JCPDS card 044-1415) as the majority phase and goethite (JCPDS card 081-0463) as the minority phase as shown in Figure 10. Thus, the structural model used for the Rietveld refinement of these XRD patterns included the crystallographic data of both phases, and in these fits, the line-broadening of diffraction peaks was analyzed with the “double-Voigt” approach.

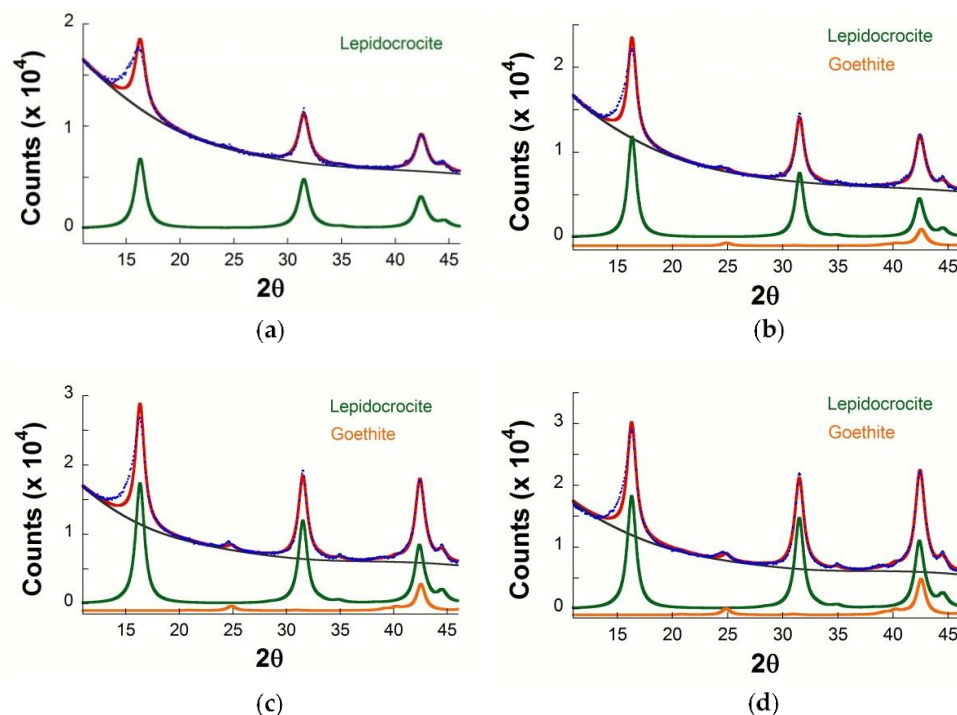


Figure 10. Comparison of the observed (blue circles) and calculated (red line) XRD patterns obtained after Rietveld refinement of the natural patinas exposed during (a) 3, (b) 6, (c) 12 and (d) 24 months. The contribution of lepidocrocite and goethite are plotted in different colors.

In Figure 10, the observed XRD data are the blue circles, and the calculated data are the red solid line. This figure includes only the results obtained for 2θ values below 47° to emphasize and highlight that the largest discrepancy between these two data sets was found for the (020) peaks. This can be observed as the calculated reflection (first red solid peak) is quite narrower than the peak measured (blue open circles). Additionally, some misfit in the positions of this peak can be observed between the measured and calculated diffraction patterns. This figure shows that both the displacement of the maximum of the diffraction peak and the asymmetry of this peak decrease as the exposure time increases.

Lepidocrocite and goethite were identified by XRD. The characterization was performed in the entire section of the patina up to the bare WS. However, only lepidocrocite was identified by Raman spectroscopy in the natural patinas (Table 5). In this case, the laser penetration is up to a few microns, and characterization refers only to the surface. Cross section analyses showed that goethite is at the inner part of the natural patina, while lepidocrocite is on the surface [34].

4. Discussion

4.1. Aesthetic Properties Evolution of the Natural Patina

As explained by Cornell and Schwertmann [35], the optical properties of iron oxides and oxi-hydroxides depend on their particle size and refractive index. In the same way, atmospheric factors, such as pollutants, climate and orientation, affect the composition and morphology of the patina, and thus the color of the metal surface exposed outdoors varies depending on the exposure atmosphere. Iron compounds synthesized in the laboratory typically have colors ranging between red and yellow. There are some studies with soils and pigments that correlate the color properties of iron oxides and oxi-hydroxides with their composition [35–39].

The samples used in these studies were purified and/or grinded with the aim of homogenization; therefore, a correlation with composition was achieved. In our work, no correlation between color and composition was found. In addition, the obtained patinas are far from the ideal conditions of previous works. They are complex, with high roughness and mixed compounds.

Color depends on particle size, turning from red to yellow for lepidocrocite when the particle grows from 0.2 to 1–2 μm [36]. The Rietveld refinement of XRD data showed the selective line broadening of the lepidocrocite peaks, which can be associated to small crystalline size or internal disorder. Although the exposure time of the patinas could give rise to changes in the size of the lepidocrocite crystallites, the mean size of this parameter from line broadening of the XRD patterns using the double Voigt approach ranged from 7 to 8 nm for the natural patinas exposed to 3 and 24 months, respectively. Therefore, the observed differences in (020) broadening between the different patinas cannot be explained by large differences in crystallite size.

Lepidocrocite is made up of anion layers of O^{2-} and OH^- arranged in a cubic close packing stacking sequence of $-\text{ABC}-\text{ABC}-$ type along the $\langle 051 \rangle$ crystallographic direction on the orthorhombic unit cell, which corresponds to the $\langle 111 \rangle$ direction of a distorted cubic cell [40]. The lack of strong chemical bonds between the layers along the [010] direction may originate a disorder in the stacking sequence parallel to this direction, thus, giving rise to the appearance of both stacking faults and twins faults. As a result from faulting in the stacking sequence, the (020) reflection shifts from the theoretical Bragg position. On the other hand, peak asymmetry is associated to twin faulting due to the limited length scale over which the structure is crystallographic homogeneous.

The reflectance spectra of the natural patina show a maximum at 630–640 nm at 12 and 24 months of atmospheric exposure (Figure 5), which is due to a decrease in the reflectance at higher wavelengths. Since there are no other oxi-hydroxides but lepidocrocite on the surface (Table 5), the changes of the reflectance spectra cannot be associated with the formation of new compounds that could be absorbing light at high wavelengths.

However, it could be associated to the decrease of the displacement of the maximum and the asymmetry of the peak (020) with the exposure time increase (Figure 10). In this way, it is possible to correlate the light absorption at the high wavelength end with the formation of a less faulting lepidocrocite. After 12 months of atmospheric exposure, the surface of the natural patina undergoes a substantial change in its texture that remains at 24 months (Figure 4c,d). The surface turns smoother, softer and more compact.

The change on the texture of the patina surface is also observed in the b^* coordinate (yellow component) (Table 3). The b^* coordinate suffers a significant decrease in its value at 12 months of atmospheric exposure. In this way, the stabilization of the b^* coordinate at 12 and 24 months to yellowish colors (value close to 20) could be an indicator of the development of a less faulting lepidocrocite on the surface of the patina.

Several authors have indicated that the appearance of WS surfaces shifts to darker colors as the exposure time increase [11,24,41,42]. In the natural patina developed on the WS samples tested in this work there was a drop of the L^* coordinate (lightness) at 6 months of atmospheric exposure, which recovered after 12 months. Travassos et al. [23] indicated that WS patinas have different appearances depending on the season. The drop of the L^* coordinate is observed during summer—the dry season in Madrid. This decrease could be related to a seasonal effect. However, no correlation with patina composition or lepidocrocite size was found.

4.2. Aesthetic Properties Evolution of Accelerated Patinas

Regarding the differences found between the natural patina and the accelerated ones, the evolution of color properties can be divided in two different groups: (1) comparable to the natural patina and (2) non-comparable.

(1) The comparable accelerated patinas compile those in which only lepidocrocite was identified at zero time, i.e., H_2SO_4 , H_2O_2 , CH_3COOH and $NaHSO_3$. These treatments are not very corrosive—in particular, H_2O_2 and CH_3COOH , which hardly generate corrosion when they are applied (see Figures S1–S4). Accordingly, the evolution of these accelerated patinas is practically the same as with the natural patina. That is the reason why L^* , a^* and b^* coordinates of the H_2O_2 and CH_3COOH accelerated patinas show very similar values to the natural patina as exposure time increase, including the decrease of the L^* coordinate at 6 months (see Tables S1 and S2). The appearance of a smooth and compact surface after 12 months of atmospheric exposure and the correlation with the reflectance spectrum and the b^* coordinate (yellow) is also observed in these patinas.

In the case of the accelerated patinas developed with H_2SO_4 and $NaHSO_3$, the application of the chemical treatment creates a thicker layer of lepidocrocite (see Figures S5–S8). The evolution of the L^* , a^* and b^* coordinates is also very similar to the natural patina. However, a different behavior is observed in the L^* coordinate as there is no decrease of its value at 6 months of atmospheric exposure (see Tables S3 and S4). Additionally, the maximum of the reflectance spectrum at 630–640 nm is defined at shorter times than in the natural patina, i.e., after 6 months of exposure instead of 12 months. The stabilization of the b^* coordinate (yellow color) occurs as well at 12 months of atmospheric exposure.

(2) The non-comparable patinas group compiles those where akaganeite and goethite were identified at time zero in addition to lepidocrocite, i.e., the $FeCl_3$, $Fe(NO_3)_3$, HCl and HNO_3 patinas. The presence of these two additional oxo-hydroxides has an effect on the color properties (see Figures S9–S16). Cornell and Schwertmann described akaganeite and goethite as yellow, with goethite being the more intense yellow-colored of all oxo-hydroxides [35,36,38]. When seen under the light of a microscope and compared to Raman spectra, both compounds show a very dark color: blackish for akaganeite and reddish for goethite (see Figures S17 and S18), which are very different from the bright colors of the lepidocrocite (see Figures S19 and S20).

The evolution of the L^* , a^* and b^* coordinates for the non-comparable patinas differs from the coordinates of the natural patina, with values that are generally lower (see Tables S5–S8). The reflectance spectra do not show a clear definition of the maximum at

630–640 nm after 24 months of atmospheric exposure, and the b^* coordinate does not show stabilization. The reasons for these differences are attributed to the effect of the additional oxo-hydroxides on the surface.

4.3. Evaluation of Color Differences and Similarities

Color differences were measured with ΔE (Equation (3)). As is seen in Figure 8 they tend to decrease with the exposure time, meaning that differences tend to reduce. There is no agreement in the literature regarding ΔE differences and their meaning. Some authors indicated that $\Delta E > 1$ represents barely perceptible differences for human eye [43], although other authors suggested that this is a misconception [26].

There are other values in the literature as $\Delta E > 2.3$ [44] to indicate whether two colors are different. Based on this previous literature, a new extended scale for color differences is proposed in Table 6. In this new scale, the accelerated patinas were classified according to ΔE values into: (i) indistinguishable ($\Delta E \leq 1$), (ii) similar ($1 < \Delta E \leq 3$), (iii) distinguishable ($3 < \Delta E \leq 5$) and (iv) different ($5 < \Delta E$), using the natural patina as a reference. However, it should be noted that this is a subjective classification based on the perception of the authors.

Table 6. Scale for classification differences in ΔE between natural patina, used as a reference, and accelerated patinas after 3, 6, 12 and 24 months of atmospheric exposure.

Classification	3 Months	6 Months	12 Months	24 Months
Indistinguishable ($\Delta E \leq 1$)	H ₂ O ₂	H ₂ O ₂	H ₂ O ₂ , CH ₃ COOH	H ₂ O ₂
Similar ($1 < \Delta E \leq 3$)	H ₂ SO ₄ , NaHSO ₃	CH ₃ COOH	H ₂ SO ₄ , NaHSO ₃	H ₂ SO ₄ , HNO ₃ , CH ₃ COOH, NaHSO ₃
Distinguishable ($3 < \Delta E \leq 5$)		NaHSO ₃		FeCl ₃ , HCl
Different ($5 < \Delta E$)	FeCl ₃ , Fe(NO ₃) ₃ , HCl, HNO ₃ , CH ₃ COOH	FeCl ₃ , Fe(NO ₃) ₃ , H ₂ SO ₄ , HCl, HNO ₃	FeCl ₃ , Fe(NO ₃) ₃ , HCl, HNO ₃	Fe(NO ₃) ₃

After 3 and 6 months of atmospheric exposure, most of the accelerated patinas are considered to be different regarding the natural patina. After six months of atmospheric exposure, there is an increase in color differences for some of the accelerated patinas (Figure 8). This change is observed due to the variation in L^* and a^* coordinates of the natural patina (Table 3), which could be attributed to a seasonal effect and a less relative humidity during summer. However, over time, the color of the accelerated patinas tends to converge to the natural patina. After 24 months of atmospheric exposure, accelerated patinas could be mostly classified as similar to the natural patina due to the low values of ΔE .

In 2001 CIE committee published a new formula for ΔE , labeled as ΔE_{00} , which solved some of the problems that the previous one had. The ΔE_{00} is more complex, and its use is not so spread due to complications in calculations. In order to know if both formulas describe the same color differences, calculations of ΔE_{00} were conducted following the methodology given in [45]. ΔE and ΔE_{00} show the same tendency over time (see Figure S21), indicating that both formulas describe a similar trend and can be used equally. The only difference between ΔE and ΔE_{00} calculation is the scale. In this way, ΔE and ΔE_{00} can be used equally in WS patinas by adjusting the values for each category in Table 6.

An alternative proposed to simultaneously compare a large number of patinas is by fitting a^* and b^* coordinates to a straight line (Equation (4)). As seen in Figure 9, there is a good fitting at 24 months of atmospheric exposure, meaning that natural and accelerated

patinas have the same hue. The slope of the lineal regression is slightly higher than 1, describing a yellowish hue for all patinas at all exposure times. Differences among patinas relate to the chroma saturation. For example, the patinas initially formed with the FeCl_3 treatment show grayish colors, and the patina of the CH_3COOH treatment presents more vivid colors.

Daukšys et al. [22] described the effect of cyclical changes of ambient temperature in the color and texture of WS rust layers. Authors performed cyclic temperature fluctuation from $+20\text{ }^\circ\text{C}$ to $-20\text{ }^\circ\text{C}$ in 24 h to WS samples, according to the climate conditions in Lithuania. In the present work, samples were exposed to the atmosphere of Madrid, described as a dry and mild weather (Figure 1). The atmospheric exposure conditions do not describe drastic temperature fluctuations, and temperatures below $0\text{ }^\circ\text{C}$ are rarely reached. For this reason, the temperature has not been considered as a determining effect for the color and texture of WS patinas.

The Pearson's coefficient indicates that there is a lineal correlation between the colors of the different patinas (Table 4). The improvement of the coefficient as well as the standard error show that the color of the patinas tends to converge to the same hue with the exposure time.

5. Conclusions

The present study shows the evaluation of the aesthetic properties of different accelerated patinas and the evolution after atmospheric exposure. The accelerated patinas were created by the application of eight chemical treatments on WS surface. Additionally, a patina developed exclusively by atmospheric corrosion, called a natural patina, was studied and taken as a reference for the accelerated patina evaluation.

The monitoring of color and composition was performed up to 24 months of atmospheric exposure. The natural patina demonstrated a smooth and compact lepidocrocite layer on the surface after 12 months of atmospheric exposure. The development of this layer correlated with the appearance of a maximum in the reflectance spectrum at 630 nm. The b^* coordinate (yellow component) can be used to monitor the development of this layer, as a stabilization of this parameter was observed after 12 months of exposure time. The comparative study of XRD patterns showed the displacement of the (020) lepidocrocite reflection and asymmetric broadening of selective lines of this phase that were associated to stacking and twins faults, respectively. These results suggest that the stacking mode of anions in the structure exerts a strong control on the properties of the outermost rust layers and therefore on the color observed.

Regarding the evolution of the aesthetic properties, the accelerated patinas were classified as comparable and non-comparable to the natural patina. For the comparable patinas (i.e., treatments with H_2SO_4 , H_2O_2 , CH_3COOH and NaHSO_3) only lepidocrocite was identified on the surface. The evolutions on the L^* , a^* and b^* coordinates were very similar to the natural patina and therefore the aesthetic properties. For the non-comparable patinas (i.e., treatments with FeCl_3 , $\text{Fe}(\text{NO}_3)_3$, HCl and HNO_3) akaganeite or goethite were identified on the surface of the patina as well as lepidocrocite. These compounds have a great influence on the aesthetic properties of the patina since a^* and b^* coordinates show lower values.

The ΔE formula was used, and a new extended classification for color differences was proposed. Additionally, a new methodology was also proposed to perform the simultaneous evaluation of color differences on a larger number of patinas. This new methodology is based on the linear fitting of a^* and b^* coordinates. The ΔE and fitting results show that the color differences of the accelerated patinas regarding the natural patina tended to decrease with exposure time. The color of the patinas converges to the same hue (a slightly yellow color), and the differences concern color saturation.

Supplementary Materials: The following supporting information can be downloaded at: <https://www.mdpi.com/article/10.3390/met12060977/s1>, Figure S1: Optical microscope images of H_2O_2 patina at different exposure times; Figure S2: Reflectance spectrum of H_2O_2 patina at different exposure times; Figure S3: Optical microscope images of CH_3COOH patina at different exposure

times; Figure S4: Reflectance spectrum of CH₃COOH patina at different exposure times; Figure S5: Optical microscope images of H₂SO₄ patina at different exposure times; Figure S6: Reflectance spectrum of H₂SO₄ patina at different exposure times; Figure S7: Optical microscope images of NaHSO₃ patina at different exposure times; Figure S8: Reflectance spectrum of NaHSO₃ patina at different exposure times; Figure S9: Optical microscope images of FeCl₃ patina at different exposure times; Figure S10: Reflectance spectrum of FeCl₃ patina at different exposure times; Figure S11: Optical microscope images of Fe(NO₃)₃ patina at different exposure times; Figure S12: Reflectance spectrum of Fe(NO₃)₃ patina at different exposure times; Figure S13: Optical microscope images of HCl patina at different exposure times; Figure S14: Reflectance spectrum of HCl patina at different exposure times; Figure S15: Optical microscope images of HNO₃ patina at different exposure times; Figure S16: Reflectance spectrum of HNO₃ patina at different exposure times; Figure S17: Akanageite section of the accelerated patina developed with FeCl₃ at zero time i.e., prior to atmospheric exposure; Figure S18: Goethite section of the accelerated patina developed with Fe(NO₃)₃ at zero time i.e., prior to atmospheric exposure; Figure S19: Light lepidocrocite section of the accelerated patina developed with H₂SO₄ after 3 months of atmospheric exposure; Figure S20: Dark lepidocrocite section of the accelerated patina developed with H₂SO₄ after 3 months of atmospheric exposure; Figure S21: (a) ΔE and (b) ΔE_{00} values comparing natural patina with accelerated patinas over time for 24-month period of atmospheric exposure; Table S1: Evolution of Lab values with 95% confidence interval as time passes for the H₂O₂ patina; Table S2: Evolution of Lab values with 95% confidence interval as time passes for the CH₃COOH patina; Table S3: Evolution of Lab values with 95% confidence interval as time passes for the H₂SO₄ patina; Table S4: Evolution of Lab values with 95% confidence interval as time passes for the NaHSO₃ patina; Table S5: Evolution of Lab values with 95% confidence interval as time passes for the FeCl₃ patina; Table S6: Evolution of Lab values with 95% confidence interval as time passes for the Fe(NO₃)₃ patina; Table S7: Evolution of Lab values with 95% confidence interval as time passes for the HCl patina; Table S8: Evolution of Lab values with 95% confidence interval as time passes for the HNO₃ patina.

Author Contributions: Conceptualization, A.C., G.P., E.C. and I.D.; methodology, A.C., G.P., J.A.J., I.L., S.M.-R., E.C. and I.D.; validation, A.C., G.P., S.M.-R. and I.D.; formal analysis, A.C., G.P., J.A.J., and I.L.; investigation, A.C., G.P. and I.L.; resources, J.A.J., I.L., S.M.-R. and E.C.; data curation, A.C., and I.L.; writing—original draft preparation, A.C. and J.A.J.; writing—review and editing, G.P., J.A.J., I.L., S.M.-R., E.C. and I.D.; visualization, A.C., G.P., J.A.J. and I.D.; supervision, G.P., J.A.J., S.M.-R., E.C. and I.D.; project administration, S.M.-R., E.C. and I.D.; and funding acquisition, E.C. All authors have read and agreed to the published version of the manuscript.

Funding: This research was funded by Agencia Estatal de Investigación, grant number BES-2015-071472; Ministerio de Economía y Competitividad, project CREMEL II (HAR2014-54893-R); and by Comunidad de Madrid and European Structural and Investment Funds, project TOP-HERITAGE CM (S2018/NMT-4372).

Data Availability Statement: Data is available at CSIC Institutional Repository: Digital CSIC (<https://digital.csic.es/>).

Acknowledgments: The authors are thankful to all the sculptors who have shared their knowledge and experience, especially to Carlos Albert, Martín Chirino and Adriana Veyrat for their kind collaboration and to the professional support of the CSIC Interdisciplinary Thematic Platform (PTI) Patrimonio Abierto: Investigación y Sociedad. (PTI-PAIS).

Conflicts of Interest: The authors declare no conflict of interest.

References

1. Murata, T.T. Weathering steel. In *Uhlig's Corrosion Handbook*, 2nd ed.; Revie, R.W., Ed.; John Wiley & Sons: Toronto, ON, Canada, 2000; pp. 621–632.
2. Morcillo, M.; Díaz, I.; Chico, B.; Cano, H.; de la Fuente, D. Weathering steels: From empirical development to scientific design. A review. *Corros. Sci.* **2014**, *83*, 6–31. [[CrossRef](#)]
3. Wang, Z.; Liu, J.; Wu, L.; Han, R.; Sun, Y. Study of the corrosion behavior of weathering steels in atmospheric environments. *Corros. Sci.* **2013**, *67*, 1–10. [[CrossRef](#)]
4. Morcillo, M.; Chico, B.; Díaz, I.; de la Fuente, D.; Alcántara, J.; Simancas, J. *La Corrosión Atmosférica del Acero al Carbono en Ambientes Costeros*, 1st ed.; Consejo Superior de Investigaciones Científicas: Madrid, Spain, 2018.

5. Cook, D.C. Spectroscopic identification of protective and non-protective corrosion coatings on steel structures in marine environments. *Corros. Sci.* **2005**, *47*, 2550–2570. [[CrossRef](#)]
6. Matsushima, I.; Ishizu, Y.; Ueno, T.; Kanazashi, M.; Horikawa, K. Effect of Structural and Environmental Factors in the Practical Use of Low-Alloy Weathering Steel. *Corros. Eng.* **1974**, *23*, 177–182. [[CrossRef](#)]
7. Morcillo, M.; Díaz, I.; Cano, H.; Chico, B.; de la Fuente, D. Atmospheric corrosion of weathering steels. Overview for engineers. Part I: Basic concepts. *Constr. Build. Mater.* **2019**, *213*, 723–737. [[CrossRef](#)]
8. Morcillo, M.; Díaz, I.; Cano, H.; Chico, B.; de la Fuente, D. Atmospheric corrosion of weathering steels. Overview for engineers. Part II: Testing, inspection, maintenance. *Constr. Build. Mater.* **2019**, *222*, 750–765. [[CrossRef](#)]
9. Bernardi, E.; Vassura, I.; Raffo, S.; Nobili, L.; Passarini, F.; de la Fuente, D.; Morcillo, M. Influence of inorganic anions from atmospheric depositions on weathering steel corrosion and metal release. *Constr. Build. Mater.* **2020**, *236*, 117515. [[CrossRef](#)]
10. Scott, J. Conservation of weathering steel sculpture. In Proceedings of the Saving the Twentieth Century: The Conservation of Modern Materials, Ottawa, ON, Canada, 15–20 September 1991.
11. Gallagher, W.P. The Performance of Weathering Steel in Sculpture. *Mater. Perform.* **2001**, *40*, 58–61.
12. Golfomitsou, S. The role of conservation in new contemporary art installations in new contexts: The case of Richard Serra's East–West/West–East in Qatar. *Stud. Conserv.* **2016**, *61*, 55–60. [[CrossRef](#)]
13. Crespo, A. Estudio de Herrumbres Aceleradas en Escultura Contemporánea de Acero Patinable. Ph.D. Thesis, Carlos III University, Madrid, Spain, 2020.
14. Pullen, D.; Heuman, J. Modern and Contemporary Outdoor Sculpture Conservation: Challenges and Advances. *GCI Newsl.* **2007**, *22*, 1–7.
15. Chemello, C.; Cano, E.; Crespo, A.; Mardikian, P.; Patterson, C. Conservation and Investigation of Cometh the Sun: A Monumental Weathering Steel Sculpture. In Proceedings of the Interim Meeting of the ICOM-CC Metals Working Group, Neuchatel, Switzerland, 2–6 September 2019.
16. Aramendia, J.; Gomez-Nubla, L.; Castro, K.; Madariaga, J.M. Structural and chemical analyzer system for the analysis of deposited airborne particles and degradation compounds present on the surface of outdoor weathering steel objects. *Microchem. J.* **2015**, *123*, 267–275. [[CrossRef](#)]
17. Aramendia, J.; Gomez-Nubla, L.; Castro, K.; Martínez-Arkarazo, I.; Vega, D.; De Heredia, A.S.L.; De Opakua, A.G.I.; Madariaga, J.M. Portable Raman study on the conservation state of four CorTen steel-based sculptures by Eduardo Chillida impacted by urban atmospheres. *J. Raman Spectrosc.* **2012**, *43*, 1111–1117. [[CrossRef](#)]
18. Aramendia, J.; Gomez-Nubla, L.; Bellot-Gurlet, L.; Castro, K.; Paris, C.; Colomban, P.; Madariaga, J.M. Protective ability index measurement through Raman quantification imaging to diagnose the conservation state of weathering steel structures. *J. Raman Spectrosc.* **2014**, *45*, 1076–1084. [[CrossRef](#)]
19. Angelini, E.; Grassini, S.; Parvis, M.; Zucchi, F. An in situ investigation of the corrosion behavior of a weathering steel work of art. *Surf. Interface Anal.* **2012**, *44*, 942–946. [[CrossRef](#)]
20. Angelini, E.; Assante, D.; Grassini, S.; Parvis, M. EIS measurements for the assessment of the conservation state of metallic works of art. *Int. J. Circuits Syst. Signal Process.* **2014**, *8*, 240–245.
21. Crespo, A.; Ramírez-Barat, B.; Díaz, I.; Cano, E. Electrochemical evaluation of the patina of the weathering steel sculpture Once Modulo. *Ge-Conservacion* **2020**, *17*, 153–159. [[CrossRef](#)]
22. Daukšys, M.; Bytautaitė, E.; Mockienė, J.; Nizevičienė, D. NaCl and Na₂SO₄ solution effect on weathering steel visual appearance when the ambient temperature changes cyclically. *Cogent Eng.* **2019**, *6*, 1659124. [[CrossRef](#)]
23. Travassos, S.J.; Tomachuk, C.R.; de Melo, H.G. EIS investigation and patina characterization of weathering steel exposed to each of the four seasons in the São Paulo metropolitan area. *Electrochim. Acta* **2019**, *325*, 134885. [[CrossRef](#)]
24. Morcillo, M.; Chico, B.; Díaz, I.; Cano, H.; de la Fuente, D. Atmospheric corrosion data of weathering steels. A review. *Corros. Sci.* **2013**, *77*, 6–24. [[CrossRef](#)]
25. Díaz, I.; Cano, H.; Crespo, D.; Chico, B.; de la Fuente, D.; Morcillo, M. Atmospheric corrosion of ASTM A-242 and ASTM A-588 weathering steels in different types of atmosphere. *Corros. Eng. Sci. Technol.* **2018**, *53*, 449–459. [[CrossRef](#)]
26. McLaren, K. The Development of the CIE 1976 (L*a*b*) Uniform Colour Space and Colour-difference Formula. *J. Soc. Dye Colour.* **1976**, *92*, 338–341. [[CrossRef](#)]
27. De Faria, D.L.A.; Venâncio Silva, S.; De Oliveira, M.T. Raman microspectroscopy of some iron oxides and oxyhydroxides. *J. Raman Spectrosc.* **1997**, *28*, 873–878. [[CrossRef](#)]
28. Criado, M.; Martínez-Ramírez, S.; Bastidas, J.M. A Raman spectroscopy study of steel corrosion products in activated fly ash mortar containing chlorides. *Constr. Build. Mater.* **2015**, *96*, 383–390. [[CrossRef](#)]
29. Villars, P.; Cenzual, K. *Pearson's Crystal Data: Crystal Structure Database for Inorganic Compounds*; ASM International: Materials Park, OH, USA, 2010.
30. Balzar, D.; Ledbetter, H. Voigt-function modeling in Fourier analysis of size- and strain-broadened X-ray diffraction peaks. *J. Appl. Crystallogr.* **1993**, *26*, 97–103. [[CrossRef](#)]
31. Morcillo, M.; de La Fuente, D.; Díaz, I.; Cano, H. Atmospheric corrosion of mild Steel. *Rev. Metal.* **2011**, *47*, 426–444. [[CrossRef](#)]
32. de la Fuente, D.; Alcántara, J.; Chico, B.; Díaz, I.; Jiménez, J.A.; Morcillo, M. Characterisation of rust surfaces formed on mild steel exposed to marine atmospheres using XRD and SEM/Micro-Raman techniques. *Corros. Sci.* **2016**, *110*, 253–264. [[CrossRef](#)]

33. Alcántara, J.; Chico, B.; Simancas, J.; Díaz, I.; de la Fuente, D.; Morcillo, M. An attempt to classify the morphologies presented by different rust phases formed during the exposure of carbon steel to marine atmospheres. *Mater. Charact.* **2016**, *118*, 65–78. [[CrossRef](#)]
34. Crespo, A.; Díaz, I.; Neff, D.; Llorente, I.; Martínez-Ramírez, S.; Cano, E. Effect of Sulfuric Acid Patination Treatment on Atmospheric Corrosion of Weathering Steel. *Metals* **2020**, *10*, 591. [[CrossRef](#)]
35. Cornell, R.M.; Schwertmann, U. *The Iron oxides: Structure, Properties, Reactions, Occurrences and Uses*, 2nd ed.; John Wiley & Sons: Weinheim, Germany, 2003.
36. Schwertmann, U.; Cornell, R.M. *Iron Oxides in the Laboratory: PREPARATION and Characterization*; John Wiley & Sons: Weinheim, Germany, 2000.
37. Scheinost, A.C.; Chavernas, A.; Barrón, V.; Torrent, J. Use and limitations of second-derivative diffuse reflectance spectroscopy in the visible to near-infrared range to identify and quantify Fe oxide minerals in soils. *Clays Clay Miner.* **1998**, *46*, 528–536. [[CrossRef](#)]
38. Scheinost, A.C.; Schwertmann, U. Color identification of iron oxides and hydroxysulfates: Use and limitations. *Soil Sci. Soc. Am. J.* **1999**, *63*, 1463–1471. [[CrossRef](#)]
39. Elias, E.; Chartier, C.; Prévot, G.; Garay, H.; Vignaud, C. The colour of ochres explained by their composition. *Mater. Sci. Eng. B Solid-State Mater. Adv. Technol.* **2006**, *127*, 70–80. [[CrossRef](#)]
40. Fasiska, E.J. Structural aspects of the oxides and oxyhydrates of iron. *Corros. Sci.* **1967**, *7*, 833–839. [[CrossRef](#)]
41. Alcántara, J.; de la Fuente, D.; Chico, B.; Simancas, J.; Díaz, I.; Morcillo, M. Marine atmospheric corrosion of carbon steel: A review. *Materials* **2014**, *10*, 406. [[CrossRef](#)]
42. Cano, H.; Neff, D.; Morcillo, M.; Dillmann, P.; Diaz, I.; de la Fuente, D. Characterization of corrosion products formed on Ni 2.4 wt%-Cu 0.5 wt%-Cr 0.5 wt% weathering steel exposed in marine atmospheres. *Corros. Sci.* **2014**, *87*, 438–451. [[CrossRef](#)]
43. Ghelardi, E.; Degano, I.; Colombini, M.P.; Mazurek, J.; Schilling, M.; Khanjian, H.; Learner, T. A multi-analytical study on the photochemical degradation of synthetic organic pigments. *Dye. Pigment.* **2015**, *123*, 396–403. [[CrossRef](#)]
44. Mahy, M.; Van Eycken, L.; Oosterlinck, A. Evaluation of Uniform Color Spaces Developed after the Adoption of CIELAB and CIELUV. *Color Res. Appl.* **1994**, *19*, 105–121.
45. Sharma, G.; Wu, W.; Dalal, E.N. The CIEDE2000 color-difference formula: Implementation notes, supplementary test data, and mathematical observations. *Color Res. Appl.* **2005**, *30*, 21–30. [[CrossRef](#)]